Flow Control in Micro-channels using Groove Orientation

A. Mohammadi[1], J.M. Floryan[1]

[1]Department of Mechanical and Materials Engineering
The University of Western Ontario, London, Ontario N6A 5B9, Canada

Abstract

This paper is focused on the analysis of changes in the flow or pressure gradient induced by surface grooves, including the effects of shape of the grooves as well as their orientation with respect to the flow. The flow has been determined using a novel grid-less spectral algorithm based on the Immersed Boundary Conditions (IBC) concept, where the boundary conditions are submerged inside the computational domain and are treated as internal constraints. The results show strong dependence of pressure losses on the groove orientation. It is possible to reduce such losses, as compared with the smooth channel, by judicious selection of groove geometry and orientation.

Introduction

Many biological systems contain surfaces exhibiting properties of interest in practical applications. Identification of special features of these surfaces are the goals of biomimetics [17] and understanding how these features are generated provides information base necessary for their mimicking in the engineering devices. Use of surface corrugations/roughness is wide spread and does not always have origin in biological systems. It is known that surface roughness affects the form of turbulence [16], it plays a large role in the laminar-turbulent transition [7] and it is used as a mixing augmentation technique in heat transfer. The following discussion is limited to a provision of a few examples of many application areas with focus on the fluid dynamic problems.

Wibel and Ehrhard [26] studied the effects of grooves on the laminar-turbulent transition in rectangular micro-channels using μPIV technique. Floryan [5] studied centrifugal instability induced by grooves in Couette flow and in Poiseuille flow [6]. Floryan and Floryan [8] considered travelling wave instability. Szumbarski and Floryan [25] studied transient growth. Asai and Floryan [1] carried out experimental verifications of theoretical predictions dealing with the effects of sinusoidal surface corrugation on the critical Reynolds number. Floryan [7] argued that the definition of hydraulic smoothness can based on the bifurcation point that determines when the flow departs from its initial, simple laminar state.

Longitudinal grooves, commonly referred as riblets, have attracted attention due to their drag reducing capabilities in turbulent flow regimes. Bechert et al [3] provided detailed experimental measurements for grooves of various shapes. Frohnapfel et al [9] provided detailed measurements of drag reduction associated with rectangular grooves. Bechert and Bartenwerfer [2] analyzed lift-up effect induced by the grooves, established the virtual origin of velocity profile and provided a possible connection between protrusion height and drag reduction. Choi et al [4] showed through direct numerical simulations of turbulent flow that drag reduction is associated with small spacing of riblets that restrict the location of streamwise vortices above the wetted surface that limits surface area exposed to the high-speed fluid flow. Goldstein et al [11] argued that drag reduction is associated with damping of the cross-flow velocity components.

The above brief discussion shows that applications of structured surfaces are very wide. These surfaces have complex geometries and their modeling represents one of the main challenges in the flow analysis. Since surface topology can potentially induce a number of instabilities, the geometry has to be modeled with high accuracy and flow equations need to be solved with high accuracy in order to be able to capture bifurcations points in a reliable manner. The classical approach, when one numerically constructs geometry models (e.g. grid generation), is very labor intensive and this makes systematic analysis of the effects of various features of surface geometry impractical. The immersed or fictitious boundaries concept offers an effective alternative. The basic idea involves the use of a regular computational domain for discretization of the field equations while the irregular flow domain is submerged inside the computational domain. No boundary conditions are imposed at the edges of the computational domain but additional relations are added in order to satisfy flow conditions at the edges of the flow domain. The field equations are solved simultaneously inside and outside of the flow domain and the physical meaning is associated only with the part of the solution which overlaps with the flow domain. This concept was first proposed by Peskin [22] in the context of cardiac dynamics and its various variants have been reviewed in [18,23]. The common limitation is the spatial accuracy, as most of these methods are based on the low-order finite-difference, finite-volume or finite-element technique [10,18,21,22,23]. The second, less known limitation is associated with the use of the local fictitious forces required to enforce the no-slip and no-penetration conditions. These forces locally affect the flow physics and this may lead to the incorrect estimates of derivatives of flow quantities, i.e., misrepresentation of the local wall shear. This problem is likely to be more pronounced in the case of methods with higher spatial accuracy.

Spectral methods provide the lowest error for spatial discretization of the field equations but are generally limited to solution domains with regular geometries. The first spectrally accurate implementation of the immersed boundary concept was developed by Szumbarski and Floryan [24] and is referred to as the Immersed Boundary Conditions (IBC) method in the rest of this discussion. This method does not use any fictitious boundaries or fictitious forces but relies on a purely formal construction of boundary constraints in order to generate the required closing relations. The construction of boundary constraints relies on the representation of the physical boundaries in the spectral space and nullifying the relevant Fourier modes. Such implementation is limited to geometries that can be represented by Fourier expansions but results in a gridless algorithm as all possible variations of boundary geometries are described in terms of the Fourier coefficients only. The additional attractiveness of this concept is associated with the precise mathematical formalism and high accuracy. The method has been implemented to study problems involving hydrodynamic instabilities induced by surface roughness [5–8,25] and has been successfully extended to two-dimensional unsteady problems [13] as well as moving boundary problems involving Laplace, biharmonic and Navier–Stokes operators [14,12,15] and also non-Newtonian fluid problem [20].

Problem Formulation

Consider flow in a channel bounded by two grooved walls extending to $\pm\infty$ in the $\hat{x}$- and $\hat{z}$-directions, where the $\hat{x}$-axis overlaps with the direction of the flow (figure 1). The grooves are

periodic with wavelengths $\lambda_{\hat{x}} = 2\pi/\hat{\alpha}$ and $\lambda_{\hat{z}} = 2\pi/\hat{\beta}$, where $\hat{\alpha}$ and $\hat{\beta}$ stand for the wave numbers in the $\hat{x}$- and $\hat{z}$-directions, respectively. Shapes of the grooves are specified as $\hat{y}_U(\hat{x},\hat{z})$ and $\hat{y}_L(\hat{x},\hat{z})$, where the subscripts *U* and *L* refer to the upper and lower walls, respectively. The grooves are inclined with respect to the flow direction with an angle $\pi/2-\phi$, i.e., the ridges form angle ϕ with the $\hat{z}$-axis (see figure 1). We shall refer to grooves corresponding to ϕ=0° as the transverse grooves, ϕ=90° as the longitudinal grooves, and ϕ between 0° and 90° as the oblique grooves. The shapes of the grooves can be expressed in terms of Fourier expansions in the form

$$\hat{y}_U(\hat{x},\hat{z}) = 1 + \sum_{n=-N_A}^{n=N_A}\sum_{m=-N_A}^{m=N_A} \hat{H}_U^{(n,m)} e^{i(n\hat{\alpha}\hat{x}+m\hat{\beta}\hat{z})}\,,$$
$$\hat{y}_L(\hat{x},\hat{z}) = -1 + \sum_{n=-N_A}^{n=N_A}\sum_{m=-N_A}^{m=N_A} \hat{H}_L^{(n,m)} e^{i(n\hat{\alpha}\hat{x}+m\hat{\beta}\hat{z})}\,, \qquad (1a,b)$$

where $\hat{H}_U^{(n,m)} = \hat{H}_U^{(-n,-m)*}$, $\hat{H}_L^{(n,m)} = \hat{H}_L^{(-n,-m)*}$, stars denote the complex conjugates, and N_A is the number of Fourier modes needed to describe groove geometry. It is convenient to introduce a different reference system $(x,\hat{y},z)$ where the *x*-axis is perpendicular and the *z*-axis is parallel to the grooves' ridges (see figure 1). The new system permits description of geometry of the grooves in terms of single Fourier expansions, i.e.,

$$\hat{y}_U(x) = 1 + \sum_{n=-N_A}^{n=N_A} H_U^{(n)} e^{in\alpha x}\,,\ \hat{y}_L(x) = -1 + \sum_{n=-N_A}^{n=N_A} H_L^{(n)} e^{in\alpha x}\,, \qquad (2a,b)$$

where $\hat{H}_U^{(n)} = \hat{H}_U^{(-n)*}$, $\hat{H}_L^{(n)} = \hat{H}_L^{(-n)*}$ and α stands for the wave number in the *x*-direction. Transformation between the $(\hat{x},\hat{y},\hat{z})$ and $(x,\hat{y},z)$ systems has the form

$$x = \cos(\phi)\hat{x} - \sin(\phi)\hat{z}\,,\ z = \sin(\phi)\hat{x} + \cos(\phi)\hat{z}\,. \qquad (3a,b)$$

Relations between coefficients of expansions (1) and (2) have the form

$$\hat{H}_U^{(n,m)} = H_U^{(n)} \text{ for } n = -m\,,\quad \hat{H}_U^{(n,m)} = 0 \text{ for } n \neq -m\,, \qquad (4a,b)$$

$$\hat{H}_L^{(n,m)} = H_L^{(n)} \text{ for } n = -m\,,\quad \hat{H}_L^{(n,m)} = 0 \text{ for } n \neq -m\,, \qquad (5a,b)$$

and relations between the wave numbers take the form

$$\hat{\alpha} = \alpha\cos(\phi)\,,\qquad \hat{\beta} = \alpha\sin(\phi)\,. \qquad (6a,b)$$

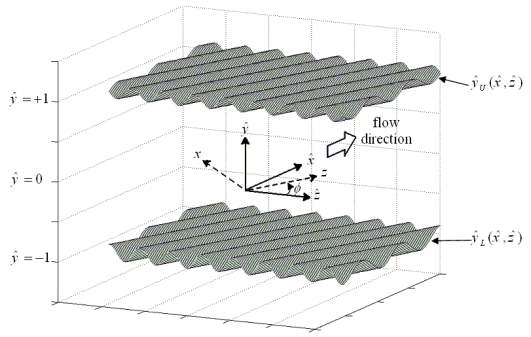

Figure 1. Channel with grooved walls. The $(\hat{x},\hat{y},\hat{z})$ coordinate system is flow-oriented and the (x,y,z) system is grooved-oriented. The angle ϕ shows the relative orientation of both systems.

Flow between smooth walls is taken as the reference flow and the direction of this flow defines the reference flow direction. This flow is driven by a constant pressure gradient directed in the negative $\hat{x}$-direction resulting in the velocity and pressure fields which in the auxiliary reference system take the form

$$\mathbf{V}_0(\hat{y}) = [u_0, v_0, w_0] = [(1-\hat{y}^2)\cos(\phi), 0, (1-\hat{y}^2)\sin(\phi)]\,, \qquad (7)$$

$$p_0(x,z) = -2Re^{-1}[x\cos(\phi) + z\sin(\phi)] + c\,, \qquad (8)$$

where $\mathbf{V}_0$ is the reference velocity vector, p_0 is the reference pressure and *c* denotes an arbitrary constant. It is advantageous to carry out numerical solution using the $(x,\hat{y},z)$-system defined by equation (3). The total velocity and pressure fields can be expressed in this system as

$$\mathbf{V}(\mathbf{x}) = [u_0(\hat{y}) + u_1(x,\hat{y}), v_1(x,\hat{y}), w_0(\hat{y}) + w_1(x,\hat{y})]\,, \qquad (9)$$

$$p(\mathbf{x}) = p_0(x,z) + p_1(x,\hat{y},z) = p_0(x,z) + h_x x + h_z z + q(x,\hat{y})\,, \qquad (10)$$

where subscripts 0 and 1 refer to the reference flow and flow modifications due to the presence of the grooves, respectively, h_x and h_z denote modifications of the mean pressure gradient in the *x*- and *z*-directions, respectively and $q(x,\hat{y})$ describes the *x*-periodic part of the pressure modification.

The flow in the auxiliary reference system is a function of only two coordinates, i.e., $(x,\hat{y})$, therefore the continuity and Navier–Stokes equations reduce to the following form

$$\partial_x u_1 + \partial_{\hat{y}} v_1 = 0\,, \qquad (11)$$

$$u_1\partial_x u_1 + v_1\partial_{\hat{y}} u_1 + v_1\hat{D}u_0 + u_0\partial_x u_1 = -h_x - \partial_x q + Re^{-1}\nabla^2 u_1\,, \qquad (12)$$

$$u_1\partial_x v_1 + v_1\partial_{\hat{y}} v_1 + u_0\partial_x v_1 = -\partial_{\hat{y}} q + Re^{-1}\nabla^2 v_1\,, \qquad (13)$$

$$u_1\partial_x w_1 + v_1\partial_{\hat{y}} w_1 + v_1\hat{D}w_0 + u_0\partial_x w_1 = -h_z + Re^{-1}\nabla^2 w_1\,, \qquad (14)$$

where $\nabla^2 = \partial^2/\partial x^2 + \partial^2/\partial\hat{y}^2$ and $\hat{D} = d/d\hat{y}$. The reader may note that equations (11)–(13) do not contain w_1 and thus they form an independent system that can be solved separately from (14). It can be shown that such separation may be carried out only for certain types of flow constraints.

In order to form a close system of equations one needs to specify two arbitrary closing conditions. Four types of conditions/constraints are of interest: fixed volume flow rate per unit width in the $\hat{x}$-direction, fixed volume flow rate per unit width in the $\hat{z}$-direction, fixed mean pressure gradient in the $\hat{x}$-direction and fixed mean pressure gradient in the $\hat{z}$-direction.

The boundary conditions take the form

$$u_1(\hat{y}_U(x)) = -u_0(\hat{y}_U(x)),\ v_1(\hat{y}_U(x)) = 0,\ w_1(\hat{y}_U(x)) = -w_0(\hat{y}_U(x)), \qquad (15a\text{-}c)$$

$$u_1(\hat{y}_L(x)) = -u_0(\hat{y}_L(x)),\ v_1(\hat{y}_L(x)) = 0,\ w_1(\hat{y}_L(x)) = -w_0(\hat{y}_L(x)), \qquad (16a\text{-}c)$$

Only when the volume flow rate constraints are chosen or when the pressure gradient constraints are chosen, equations. (11)–(13) with boundary conditions (15a,b) and (16a,b) become independent of w_1 and can be solved separately. Their solution describes a two-dimensional motion in the $(x,\hat{y})$ plane. The flow in the *z*-direction can be determined in the second step of the solution process by solving equation (14) with the boundary conditions (15c) and (16c). If the flow rate and pressure gradient constraints are mixed, the decoupling does not occur and one needs to solve equations (11)–(14) as a single system.

Discretization and Solution Process

The enforcement of boundary conditions is based on the IBC concept which relies on the use of a fixed computational domain extending in the $\hat{y}$-direction far enough so that it completely encloses the grooved channel [24]. The solution is assumed to be periodic in the *x*-direction and thus all unknowns can be expressed using Fourier series. Chebyshev polynomials are used for discretization in the *y*-direction. The boundary conditions are

enforced on the surface of the grooves using the IBC concept which their implementation is explained in [24].

The solution process consists of two steps, i.e., solution of the nonlinear problem (equations (11)–(13)) to determine flow in the (x,y) plane and the follow up solution of the linear problem (equation (14)) to determine flow in the z-direction where the details are described in [19].

Numerical Results

Presence of transverse grooves increases flow resistance and reduces the volume flow rate for a fixed pressure gradient (and equal to the reference flow pressure gradient). The volume flow rate changes as a function of the grooves' orientation. As the grooves rotate away from the transverse position and become more aligned with the direction of the imposed pressure gradient ($\hat{x}$-direction), the flow resistance decreases leading to an increase in the volume flow rate. Results shown in figure 2 demonstrate that the maximum flow rate (minimum resistance) in the direction of pressure gradient ($\hat{x}$-direction) corresponds to the grooves assuming longitudinal orientation (ϕ=90°). As the grooves rotate away from this position, they force a net flow in the spanwise direction ($\hat{z}$-direction). The maximum of this flow occurs for $\phi \approx 42°$ depending on the groove wave number and amplitude, and decreases to zero as the grooves approach the transverse orientation (ϕ=0°). Grooves with higher wave numbers and higher amplitudes are more effective in creating spanwise flow. Similarly, effectiveness of these grooves increases with an increase of the Reynolds number Re. It is interesting to observe that in the case of longitudinal grooves (ϕ=90°), u_0=0, v_1=0, u_1=0, $\nabla^2 w_1$=0 and the flow modifications are unidirectional and independent of the Reynolds number.

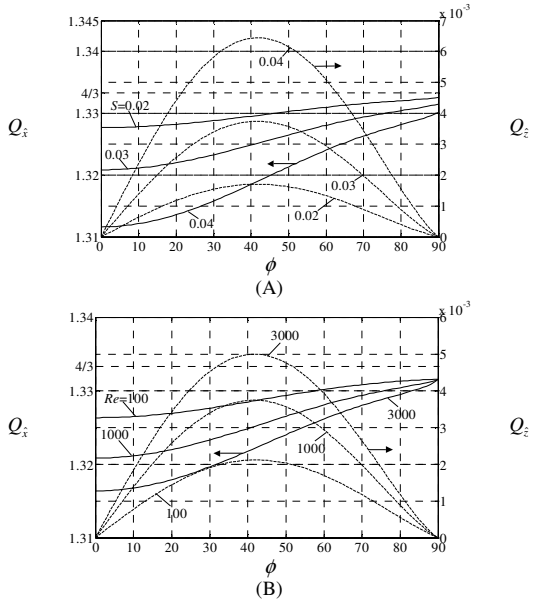

Figure 2. Variations of the volume flow rate per unit width $Q_{\hat{x}}$ in the reference flow direction ($\hat{x}$-direction, solid lines) and of the volume flow rate $Q_{\hat{z}}$ in the orthogonal direction ($\hat{z}$-direction, dash lines) as a function of the groove inclination angle ϕ. Figure 2A– Re=1000, α=3 and typical values of the groove amplitude S. Figure 2B – α=3, S=0.03 and typical values of the flow Reynolds number Re.

Similar calculations have been carried out for the case of fixed flow rates constraints (flow rate was assumed to be equal to that given by the reference flow). Variations of the additional pressure gradients required to maintain such flow rates are plotted in figure 3 as a function of the grooves' orientation angle ϕ. Presence of the transverse grooves (ϕ=0°) results in an increase of the flow resistance and therefore an additional pressure gradient needs to be added to maintain the same flow rate. As the grooves rotate away from the transverse position and become more aligned with the direction of the reference flow ($\hat{x}$-direction), the flow resistance decreases. The minimum resistance and thus the minimum additional pressure gradient corresponds to the grooves assuming longitudinal orientation (ϕ=90°). Presence of oblique grooves creates tendency for the flow to follow direction of the grooves. Spanwise pressure gradient must be added in order to prevent net flow in the spanwise direction. This situation would occur in a channel with a finite spanwise width as the side walls would prevent any net flow in the spanwise direction. The side walls would be exposed to pressure forces associated with the spanwise pressure gradient required to eliminate the spanwise flow. The maximum spanwise pressure gradient occurs for $\phi \approx 42°$ depending on the groove wave number and amplitude, and decreases to zero as the grooves approach either the transverse and or the longitudinal orientations. Grooves with higher wave numbers α and higher amplitudes S require higher additional pressure gradients in order to maintain the same flow rates. Increase of the flow Reynolds number Re increases the pressure correction factors $Re \times h_{\hat{x}}$ and $Re \times h_{\hat{z}}$. In the case of longitudinal grooves (ϕ=90°), $Re \times h_{\hat{x}}$ becomes independent of the flow Reynolds number Re.

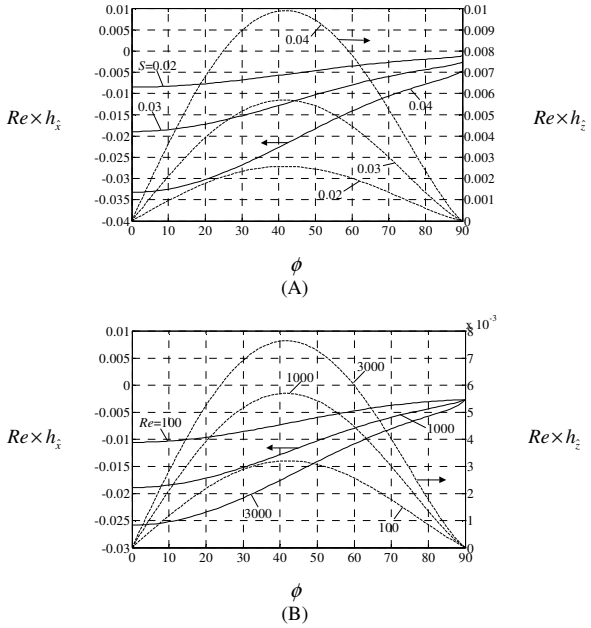

Figure 3. Variations of the pressure correction factors $Re \times h_{\hat{x}}$ (solid lines) and $Re \times h_{\hat{z}}$ (dash lines) as functions of the groove inclination angle ϕ. Figure. 3A– Re=1000, α=3 and typical values of the groove amplitude S. Figure. 3B – α=3, S=0.03 and typical values of the flow Reynolds number Re.

Conclusions

A spectral algorithm suitable for analysis of flows in channels with grooved walls has been presented. The grooves are two-dimensional but may have arbitrary orientation with respect to the reference flow direction. This direction is defined as the flow direction when grooves are absent. In the case of transverse grooves the flow is two-dimensional; the flow becomes three-dimensional for oblique grooves and remains three-dimensional when grooves assume longitudinal orientation. The algorithm models geometry of the grooves using Fourier expansions.

Computations are carried out in a fixed computational domain with the grooves submerged inside this domain. The flow boundary conditions are enforced using the immersed boundary conditions (IBC) method which results in the construction of constraints that provide closing conditions for the field equations. The algorithm eliminates the need for costly coordinate generation and provides flexibility required for an efficient analysis of various possible grooves' geometries.

Presence of transverse grooves increases flow resistance and reduces the volume flow rate for a fixed pressure gradient. The volume flow rate changes as a function of the grooves' orientation. The maximum flow rate (minimum resistance) in the direction of pressure gradient ($\hat{x}$ -direction) corresponds to the grooves assuming longitudinal orientation (ϕ=90°). Grooves with higher wave numbers and higher amplitudes are more effective in creating spanwise flow. The maximum of this spanwise flow occurs for $\phi \approx 42°$. Similarly for the case of fixed flow rates constraints, presence of the transverse grooves (ϕ=0°) results in an increase of the flow resistance and therefore an additional pressure gradient needs to be added to maintain the same flow rate. The minimum resistance and thus the minimum additional pressure gradient corresponds to the grooves assuming longitudinal orientation (ϕ=90°).

The novel algorithm developed as a part of this study permits efficient optimization of grooves' shape and orientation that leads to either maximization or minimization of pressure drop associated with the flow.

Acknowledgments

This work has been carried out with support of SHARCNET and NSERC of Canada. SHARCNET of Canada provided computing resources. The authors would like to acknowledge discussions with Dr.J.Szumbarski on the subject of the presented algorithm.

References

[1] Asai, M. & Floryan, J.M., Experiments on the Linear Instability of Flow in a Wavy Channel, *Eur. J. Mech. B/Fluids*, **25**, 2006, 971–986.

[2] Bechert, D.W. & Bartenwerfer, M., The Viscous Flow on Surfaces with Longitudinal Ribs, *J. Fluid Mech.*, **206**, 1989, 105–129.

[3] Bechert, D.W., Bruse, M., Hage, W., Van Der Hoeven, J.G.T., & Hoppe, G., Experiments on Drag-Reducing Surfaces and Their Optimization with an Adjustable Geometry, *J. Fluid Mech.*, **338**, 1997, 59–87.

[4] Choi, H., Moin, P. & Kim, J., Direct Numerical Simulation of Turbulent Flow over Riblets, *J. Fluid Mech.*, **255**, 1993, 503–539.

[5] Floryan, J.M., Centrifugal Instability of Couette Flow over a Wavy Wall, *Phys. Fluids*, **14**, 2002, 312–322.

[6] Floryan, J.M., Vortex Instability in a Converging-Diverging Channel, *J. Fluid Mech.*, **482**, 2003, 17–50.

[7] Floryan, J.M., Three-dimensional Instabilities of Laminar Flow in a Rough Channel and the Concept of Hydraulically Smooth Wall, *Eur. J. Mech. B/Fluids*, **26**, 2007, 305–329.

[8] Floryan, J.M. & Floryan, C., Travelling Wave Instability in a Diverging-Converging Channel, *Fluid Dyn. Res.*, **42**, 2010, 025509.

[9] Frohnapfel, B., Jovanović, J. & Delgado, A., Experimental Investigations of Turbulent Drag Reduction by Surface-Embedded Grooves, *J. Fluid Mech.*, **590**, 2007, 107–116.

[10] Girault, V., Glowinski, R. & Pan, T.W., A Fictitious-Domain Method with Distributed Multiplier for the Stokes Problem, *Appl. Nonlinear Anal.*, Springer, 2000, 159–174.

[11] Goldstein, D., Handler, R. & Sirovich, L., Direct Numerical Simulation of Turbulent Flow over a Modeled Riblet Covered Surface, *J. Fluid Mech.*, **302**, 1995, 333–376.

[12] Husain, S.Z. & Floryan, J.M., Gridless Spectral Algorithm for Stokes Flow With Moving Boundaries, *Comput. Methods Appl. Mech. Engrg.*, **198**, 2008, 245–259.

[13] Husain, S.Z. & Floryan, J.M., Immersed Boundary Conditions Method for Unsteady Flow Problems Described by the Laplace Operator, *Int. J. Numer. Meth. Fluids*, **56**, 2007, 1765–1786.

[14] Husain, S.Z. & Floryan, J.M., Implicit Spectrally-Accurate Method for Moving Boundary Problems Using Immersed Boundary Conditions Concept, *J. Comput. Phys.*, **227**, 2008, 4459–4477.

[15] Husain, S.Z. & Floryan, J.M., Spectrally-Accurate Algorithm for Moving Boundary Problems for the Navier-Stokes Equations, *J. Comput. Phys.*, **229**, 2010, 2287–2313.

[16] Jimenez, J., Turbulent Flows over Rough Walls, *Ann. Rev. Fluid Mech.*, **36**, 2004, 173–196.

[17] Jung, Y.C. & Bhushan B., Biomimetic Structures for Fluid Drag Reduction in Laminar and Turbulent Flows, *J. Phys.: Condens. Matter*, **22**, 2010, 035104 1–9.

[18] Mittal, R. & Iaccarino, G., Immersed Boundary Methods, *Annu. Rev. Fluid Mech.*, **37**, 2005, 239–261.

[19] Mohammadi, A. & Floryan, J.M., Spectral Algorithm for Analysis of Flows in Grooved Channels, Expert Systems in Fluid Dynamics Research Laboratory Report ESFD–1/2010. Department of Mechanical and Materials Engineering, The University of Western Ontario, London, Ontario, N6A 5B9.

[20] Mohammadi, A., Floryan, J.M. & Kaloni P.N., Spectrally Accurate Method for Analysis of Stationary Flows of Second-Order Fluids in Rough Micro-Channels, *Int. J. Numer. Meth. Fluids*, 2010, DOI: 10.1002/fld.2269.

[21] Parussini, L., Fictitious Domain Approach via Lagrange Multipliers with Least Squares Spectral Element Method, *J. Sci. Comput.*, **37**, 2008, 316–335.

[22] Peskin, C.S., The Fluid Dynamics of Heart Valves: Experimental, Theoretical and Computational Methods, *Annu. Rev. Fluid Mech.*, **14**, 1981, 235–259.

[23] Peskin, C.S., The Immersed Boundary Method, *Acta Numerica*, **11**, 2002, 479–517.

[24] Szumarski, J. & Floryan, J. M., A Direct Spectral Method for Determination of Flows over Corrugated Boundaries, *J. Comput. Phys.*, **153**, 1999, 378-402.

[25] Szumbarski, J. & Floryan, J.M., Transient Disturbance Growth in a Corrugated Channel, *J. Fluid Mech.*, **568**, 2006, 243–272.

[26] Wibel, W. & Ehrhard P., Experiments on the Laminar/Turbulent Transition of Liquid Flows in Rectangular Micro Channels, *Proceedings of the Fifth International Conference on Nanochannels, Microchannels and Minichannels*, June 18–20, 2007, Mexico, ICNMM2007 1–8.